Direct three-dimensional coherently scattered x-ray microtomography

Congwu Cui
Department of Medical Physics, CancerCare Manitoba, 675 McDermot Avenue, Winnipeg, Manitoba R3E 0V9, Canada

Steven M. Jorgensen, Diane R. Eaker, and Erik L. Ritman[a)]
Department of Physiology and Biomedical Engineering, Mayo Clinic, 200 First Street Southwest, Alfred Building 2-409, Rochester, Minnesota 55905

(Received 29 March 2010; revised 25 October 2010; accepted for publication 27 October 2010; published 18 November 2010)

Purpose: It has been shown that coherently scattered x rays can be used to discriminate and identify specific components in a mixture of low atomic weight materials. The authors demonstrated a new method of doing coherently scattered x-ray tomography with a thin sheet of x ray.
Methods: A collimated x-ray fan-beam, a parallel polycapillary collimator, and a phantom consisting of several biocompatible materials of low attenuation-based contrast were used to investigate the feasibility of the method. Because of the particular experimental setup, only the phantom translation perpendicular to the x-ray beam is needed and, thus, there is no need of Radon-type tomographic reconstruction, except for the correction of the attenuation to the primary and scattered x rays, which was performed by using a conventional attenuation-based tomographic image data set. The coherent scatter image contrast changes with momentum transfer among component materials in the specimen were investigated with multiple x-ray sources with narrow bandwidth spectra generated with anode and filter combinations of Cu/Ni (8 keV), Mo/Zr (18 keV), and Ag/Pd (22 keV) and at multiple scatter angles by orienting the detector and polycapillary collimator at different angles to the illuminating x ray.
Results: The contrast among different materials changes with the x-ray source energy and the angle at which the image was measured. The coherent scatter profiles obtained from the coherent scatter images are consistent with the published results.
Conclusions: This method can be used to directly generate the three-dimensional coherent scatter images of small animal, biopsies, or other small objects with low atomic weight biological or similar synthetic materials with low attenuation contrast. With equipment optimized, submillimeter spatial resolution may be achieved.
[DOI: 10.1118/1.3517194]

Key words: coherent x-ray scatter, computed tomography, energy-resolved x-ray detection, quasimonochromatic x-ray sources, polycapillary x-ray optics

I. INTRODUCTION

Coherently scattered x ray has the same photon energy as the illuminating x-ray photons, whereas incoherently scattered x-ray and fluorescent x-ray photons have lower x-ray photon energy than the illuminating x-ray photons.[1] The coherent scatter conveys information about chemical bonds rather than just atomic number, the mechanism underlying conventional x-ray attenuation-based imaging, due to the interference between the x rays coherently scattered by the atoms separated by the chemical bonds. Coherent scatter can, therefore, in principle, differentiate between different chemical materials even though the atomic numbers are very similar and cannot be easily distinguished by attenuation-based x-ray imaging.

The coherent scattering is described by the effective cross section of the materials,[2]

$$\frac{d\sigma}{d\Omega}(\theta) = r_e^2/2(1+\cos^2\theta)F^2(q,Z), \tag{1}$$

where θ is the scattering angle, r_e is the classical electron radius (2.82×10^{-15} m), $F^2(q,Z)$ is the molecular structural form factor, and q is the momentum transfer of the coherently scattered photons expressed as

$$q = \frac{\sin(\theta/2)}{\lambda}, \tag{2}$$

where λ is the x-ray wavelength in angstroms (Å). If a polychromatic x-ray source is used to illuminate the specimen, then the cross-section function can be measured with an energy-selective x-ray detector at a fixed angle because the range in θ can be provided by the range in photon energies (E) (keV) via $\lambda = 12.3/E$.[3] In amorphous materials and fluids, the spatial arrangement of atoms is disordered in long range so that the scattered x rays spread over a range of angles about the illuminating beam[4] rather than as sharp rings or dots as it does in powdered crystalline[5] or single crystalline[6] materials, respectively. In bioengineering and biomedical applications, some materials are made of polymers that have somewhat longer ordering range, but most materials fall into the amorphous and fluid categories. Because the coherently

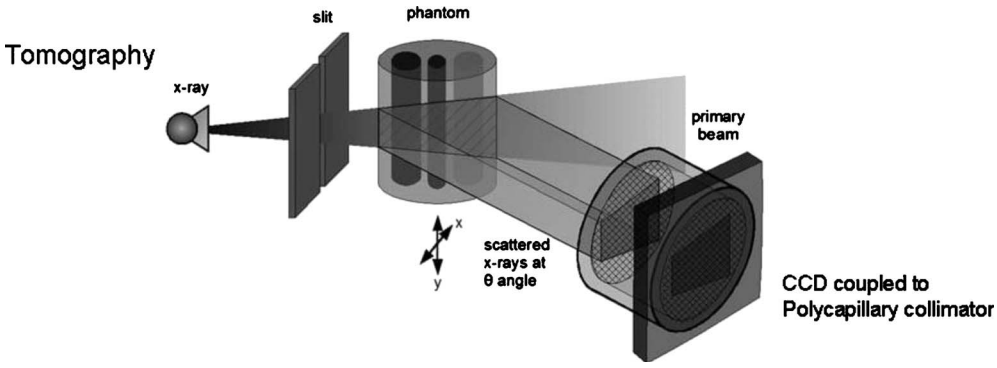

FIG. 1. Experimental setup of direct coherently scattered x-ray tomography. An x-ray cone beam is collimated with a slit aperture to form a thin fan beam. The scattered rays emerging from all points in the cross section of the beam and the object are collimated by the multichannel polycapillary collimator and then recorded by an array detector, such as a CCD. The object is translated in the x direction perpendicular to the x-ray beam. [Reproduced with permission from C.-W. Cui, S. M. Jorgensen, D. R. Eaker, and E. L. Ritman, Proc. SPIE 7078, 70781S (2008).]

scattered x-ray provides a "characteristic" of the molecular structures of the material, the coherent x-ray scattering pattern can be used to identify a specific component in a complex material.

Because biomedical synthetic materials often consist of composites that have similar densities, the contrast between x-ray attenuations of real tissue and tissue scaffolds (made of biocompatible materials) is often low and therefore hard to image by conventional attenuation-based x-ray methods. However, the different x-ray photon coherent scatter characteristics of two materials make it possible to get sufficiently high contrast between two different materials that differ little in the attenuation contrast.

Coherently scattered x-ray imaging has been studied by a number of investigators over the past two decades.[7–16] One major impediment toward routine use of coherent scatter imaging has been the use of a pencil-beam x ray, which leads to the need of both scanning transaxially and rotation at small angular increments. The feasibility of coherent scatter tomography using a fan-beam x-ray has been explored.[17–21] In this approach, a fan-beam, a collimated detector, and long tungsten lamellas are used to collect the scatter in a wide scatter angle range simultaneously. While being fairly straightforward to implement, the configuration lacks flexibility because the lamella collimator, the detector, and the x-ray source are highly correlated and it can only be used in applications with relatively large regions of the same material within an object because the recorded line integral of scatter is then predominately through one substance. For submillimeter applications, the high precision collimator, crucial to the resolution, is difficult to fabricate. Also, since the signal to noise ratio is relatively low, averaging pixels improves image quality but, in order to minimize partial volume effect, requires large areas of similar material and thus decreases spatial resolution of the image. Our method, however, does not require that as it images scatter emanating from small areas of the material.

To image the coherent scatter from different component materials in a complex object (e.g., a complex tissue or a small animal), a collimator is necessary to deconvolve the scatters from the neighboring regions. Decoupling the correlation between the collimator and the source is critical for designing high precision collimator for high spatial resolution and small objects. A parallel beam and a parallel collimator will greatly reduce the complexity.

In this paper, we demonstrate a method that uses a parallel multichannel polycapillary collimator[22] to generate three-dimensional images directly. By using a thin x-ray fan beam and a polycapillary collimator, only transaxial translation of the x-ray beam through the object is needed. The coherently scattered x rays are measured at either selected scatter angles with a monochromatic or a quasimonochromatic x-ray source or at a fixed angle with a polychromatic x-ray source with an energy dispersive array detector.

II. METHODS AND MATERIALS

Our experimental setup is shown in Fig. 1. An x-ray cone beam is generated by an x-ray tube with a specified anode material and filter. The cone beam is collimated with a slit to form a fan-beam. The scattered x rays in the cross section of the x-ray beam and the object meet an array of parallel collimators provided by a polycapillary x-ray optic and then measured by an array detector, e.g., CCD or x-ray flat panel. The collimator accepts only those x rays falling within the angle of acceptance of the device. To obtain a three-dimensional coherent scatter image of the object, the object is translated across the x-ray beam along the x direction, as shown in Fig. 1.

To minimize the complexity, a parallel beam is desirable. While it is easy to acquire an essentially parallel x-ray beam with synchrotron radiation,[23] it is not trivial with traditional x-ray sources that mostly generate cone beams, although a cone-to-parallel converting polycapillary x-ray optic could be used to accomplish this with point-source x-ray sources.[24] However, a fan-beam can be used if the object is small and far away from the source so that the beam can be treated as a quasiparallel beam. For a fan-beam, the recorded scatter

x rays corresponding to the incident x rays away from the central ray of the fan-beam have higher scatter angles. The true scatter angle (θ) at those locations is

$$\theta = a\cos(\cos(\phi)\cos(\eta)), \quad (3)$$

where ϕ is the nominal scatter angle at the center of the fan-beam and η is the half fan-angle at the point where the incident x ray is scattered. For a typical small object of 2 cm in diameter, if the fan-beam divergence is 2° (which corresponds to a source-object distance of 115 cm), at ϕ=2°, the maximum difference between θ and ϕ is 0.06°. This is tolerable for small object imaging with x-ray sources at 20 keV.

In our experiment shown in Fig. 1, the x-ray beam was collimated with a vertical slit (150 μm wide) to generate a fan-beam. The slit housing was aluminum with tungsten blades. The source-object distance was 115 cm. The slit to object center was 43 mm and the beam width at the object was 220 μm. The detector pixels were 20 μm^2. The imaging array is 1340×1300; however, only a small portion of the array actually had data because of the angle of detector array plane to scattered data. The CCD detector was fiber-optically coupled; hence, a fixed detector pixel size. The scattered x rays at the cross section of the phantom and the beam were collimated by a polycapillary collimator coupled to a CCD, which was oriented at 7.3°, 9°, and 12.2° angles to the primary x-ray beam (see Fig. 1, "scattered x rays at θ angle," for clarification). The distance between the collimator front surface and the phantom was about 20 cm. The optic was 25 mm in diameter and consisted of a 2.7cm long bundle of ~907 000 closely packed 27 μm channel diameter hollow boron glass capillaries.

To fully identify a material and to observe the change of contrast with the momentum transfer, the coherent scatter images need to be measured at different momentum transfer q. Because of the limit of our current equipment, it is inconvenient to frequently reorient the collimator and detector assembly. Therefore, we used three different x-ray source anodes and appropriate foil filters (copper/nickel, molybdenum/zirconium, and silver/palladium) to obtain three quasimonochromatic x-ray illuminating beams centered on the 8, 17.5, and 22 keV K_α emission lines of the respective anodes.[25] The measured x-ray spectra are shown in Fig. 2. At each x-ray energy, the collimator and detector were oriented to three scatter angles (12.2°, 9.0°, and 7.3°, respectively).

The phantom used is a cylinder of 2 cm in diameter and 2.5 cm in length made of lucite. It consisted of several materials, i.e., nylon, polycarbonate, polycaprolactone (PCL), water, propylene fumarate, and olive oil, with similar x-ray attenuation contrast.

During the measurement of the three-dimensional coherent scatter image, multiple contiguous slices in the vertical direction were obtained, while the object is translated across the illuminating x-ray beam in the direction perpendicular to the x-ray beam (Fig. 1). By orienting the collimator/CCD system at different angles and using the three different x-ray photon energies, the scattered x rays at multiple momentum transfers were recorded for each voxel within each illuminated plane. The exposure time for each 103 translation steps

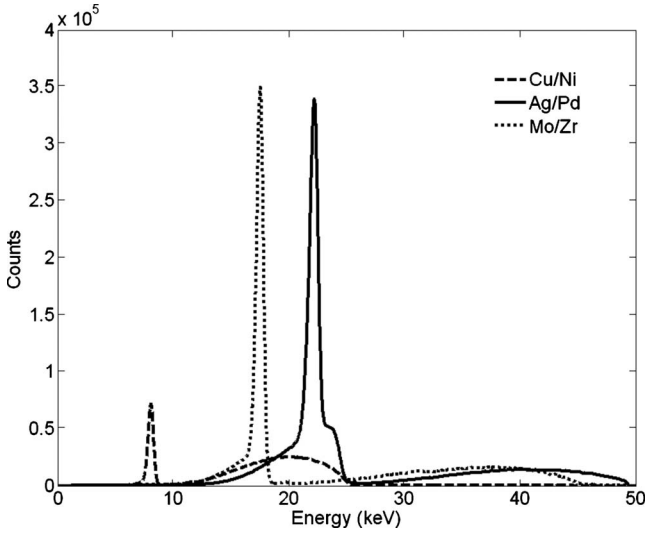

FIG. 2. The spectra of the x-ray sources used in experiment. Note: The spectra are generated with anode and filter combinations of copper/nickel, molybdenum/zirconium, and silver/palladium, respectively. An energy dispersive detector (AMPTEK Inc., Bedford, MA, model: XR-100T-CdTe) was used to measure the spectra.

was 60 min and the peak voltage and x-ray current per anode/filter were as follows: Ag/Pd, 50 kVp, 30mA; Mo/Zr, 45 kVp, 60 mA; and Cu/Ni, 25 kVp, 50 mA.

The attenuation of the object to both the primary and the scattered x rays was corrected with an attenuation CT image. The attenuations of voxels along the path of both the incident x rays and the scattered x rays were summed and then the transmissions calculated with the total attenuations were used to correct the intensities of coherent scatter signal. The attenuation images were generated with the same three x-ray source anodes as stated above for the scatter experiment. The exposure time per view was 10 s.

In our data processing, the Compton scatter and multiple scatter were not considered. It has been shown that coherent scatter in biotissue materials dominates in the low angle range and drops rapidly with increasing angle, while Compton scatter mainly happens at higher angles.[18] At low angles, both Compton scatter and multiple scatter can be treated as a low frequency background.

III. RESULTS

The coherent scatter profiles of scatter intensity versus momentum transfer of several of the materials used were generated by a conventional method so as to provide the "truth" for comparison to our phantom data. The experimental setup is show in Fig. 3. The generated profiles are shown in Fig. 4. They were generated with a pencil beam by collimating the x-ray source to a 100 μm diameter pencil beam that transilluminated the 125 μm thick sheet of the material (nylon, polycarbonate, lucite, and PCL). Water's momentum transfer was obtained from the published data.[26]

X-ray sources with Mo and W anode were used in these experiments. The Mo source was operated at 35 kVp and 60 mA. The W source was operated at 60 kVp and 40 mA. A Zr

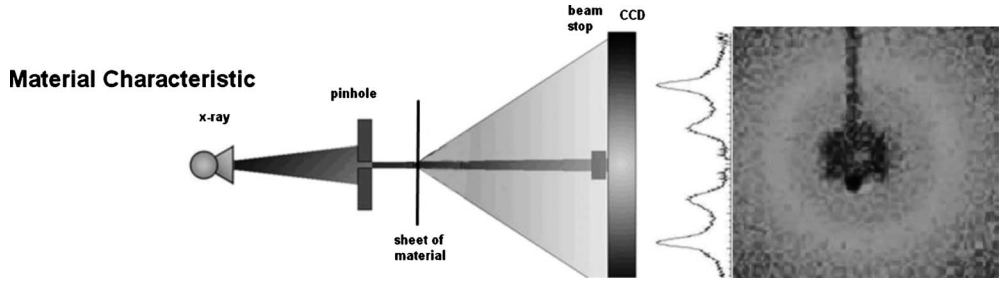

FIG. 3. Experimental setup of direct coherently scattered x-ray data collection. An x-ray cone beam is collimated with a pinhole aperture to form a pencil beam. The scattered rays emerging from all points in the thin sheet of the selected material transversed by the scatter about the pencil beam were recorded by a CCD array. [Left schematic is modified and reproduced with permission from C.-W. Cui, S. M. Jorgensen, D. R. Eaker, and E. L. Ritman, Proc. SPIE 7078, 70781S (2008).]

filter for the Mo tube and a filter set of a 75 μm Hf foil and a 254 μm Gd foil for the W tube were used, respectively, to suppress the lower and higher energy radiation. The data were corrected by subtracting the background. The radial distribution of the scatter about the x-ray pencil beam was used to generate the momentum transfer profiles.[27]

The coherent scatter images of the phantom were measured at multiple momentum transfers. Figure 21 of Ref. 28 shows the slices of the transaxial attenuation (right upper panel) and two coherent scatter (lower panels) images of the phantom, and the left upper panel shows the materials and their location in the phantom. The coherent scatter images are of axial slices coplanar with the x-ray fan beam. The attenuation of both the primary beam and the scattered x rays by the specimen was corrected with the use of the attenuation CT image of the phantom.

The attenuation images were acquired using our custom-made micro-CT scanner.[29] The detector was a CsI(Tl) crystal plate lens coupled to a CCD imaging array. The acquisition was, in 1° increment, 360° and reconstructed using a modified Feldkamp cone beam algorithm. The units of attenuation are cm^{-1}.

The coherent scatter intensities, corresponding to the scatter cross sections, of the materials from all nine data sets were combined to form the scatter profiles. Of them, the profiles of nylon, polycarbonate, lucite, water, and PCL are shown in Fig. 4. The data generated with the pencil beam as described above, which we consider to be the truth, is also plotted and compared to these results. The locations in the phantom are located in the left upper panel of Fig. 5.

IV. DISCUSSION

The coherent scatter profiles of nylon, polycarbonate, lucite, polycaprolactone, and water are compared to our truth data in Fig. 4. To facilitate comparison to the truth data, the data from our acquisitions were scaled by some factors in the three figures above so that the momentum transfer profiles

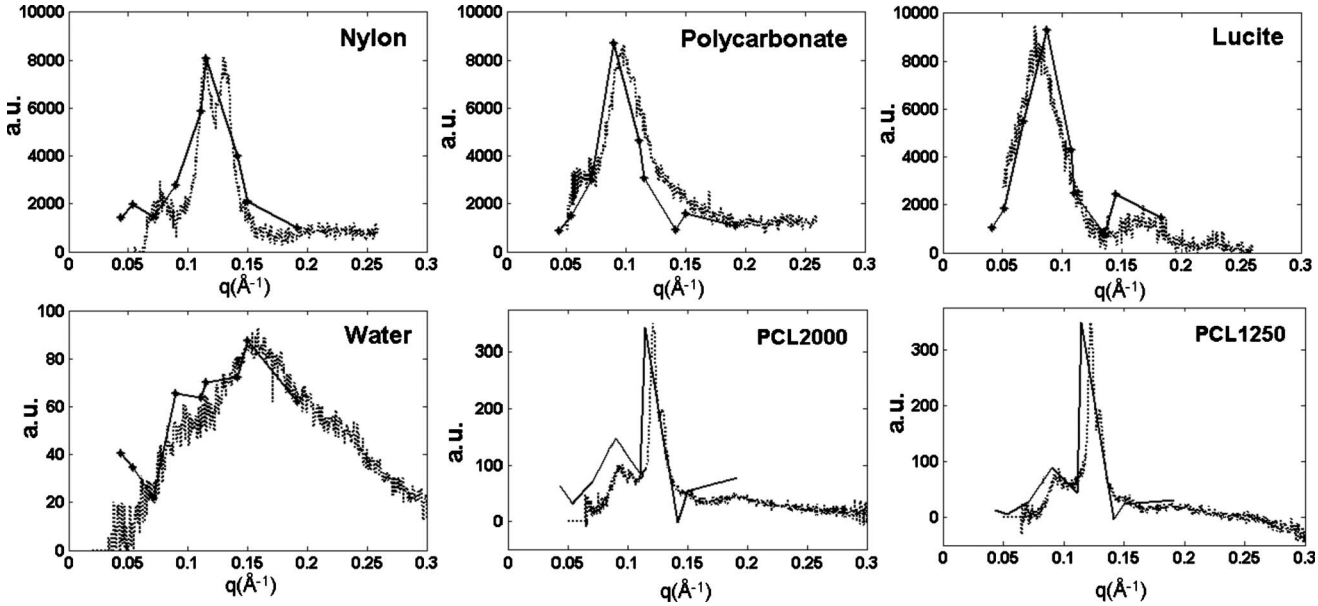

FIG. 4. Coherent scatter profiles of nylon, polycarbonate, lucite, PCL, and water obtained from scatter images measured at multiple momentum transfers. The published momentum transfer profile for water was compared to that of Ref. 26. The solid lines are data generated from our coherent scatter x-ray experiment (setup shown in Fig. 1) and the dotted lines are from the pencil-beam experiment (setup shown in Fig. 3), which we used to generate the truth data.

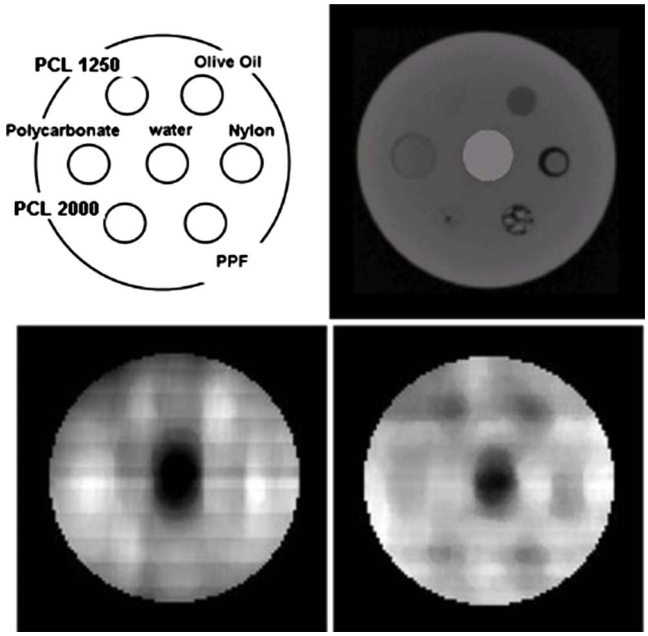

FIG. 5. Coherent scatter and attenuation images. The left upper panel is a schematic of the materials and their location in a transaxial slice of the phantom. The right upper panel is a slice of the attenuation CT image, the lower two panels, from left to right, are the transaxial slices of the coherent scatter images measured at $q=0.15$ and 0.11 $Å^{-1}$, respectively. The right upper panel was windowed from −500 to −50 Hounsfield units (HU). The HU for the materials in the micro-CT image of the test phantom are as follows: water=0, nylon=−276, polycarbonate=−260, PCL2000=−246, PCL1250=−252, and lucite=−191. The lower two panels from left to right were windowed from 0 to 3.147 and 0.292 to 8.3 arbitrary scatter values, respectively. The mean ± SD for water in a region-of-interest of the right lower panel image was 1.753 ± 0.101 arbitrary units. [Modified with permission from R. A. de Kemp, F. H. Epstein, C. Catana, B. M. W. Tsui, and E. L. Ritman, J. Nucl. Med. 51, 18S-32S (2010) (upper right and lower panels).]

would have a scale similar to the published data. Our data are consistent with other published results. The lower two panels show coherent scatter images in Fig. 5, corresponding to moment transfers of 0.15 and 0.11 $Å^{-1}$, respectively. Note that there are some distortions along the vertical direction in the shape of the materials in the $q=0.11$ $Å^{-1}$ image. Probably it is due to the misaligned collimator and detector assembly to the scattered x rays. It is difficult to accurately align, especially at low angles, the collimator and detector surfaces with our current equipment.

In the coherent scatter images, it can be seen that the contrast of the materials changes with the momentum transfer through either x-ray energy or the scatter angle. For example, the scatter intensity changes in polycarbonate, nylon, lucite, and PCL are all consistent with their single material scatter properties, as shown in Fig. 4. Therefore, the material of a single voxel can be identified either with polychromatic x-ray source by measuring scatter at a fixed angle or with a monochromatic x-ray source by measuring scatter at multiple scatter angles. By orienting the detector to a specific scatter angle and using a monochromatic x-ray source, a material can be identified to be present or absent. For all its potential advantages, the use of coherent scatter for imaging presents several technical challenges in its implementation.

This approach is very inefficient in measuring the coherent scatter. The coherent scatter is circularly symmetric around the illuminating beam. With the multiple channel parallel collimators, only a very small fraction of the scatter is measured. Therefore, long exposure time or high fluence x-ray source is needed to get sufficient signal. Bringing the x-ray source closer to the detector can reduce exposure time by 1/distance^2, but it should be far enough such that the focal spot is less than the fan beam thickness. Also, increasing the slit width can reduce exposure time at the price of spatial resolution (i.e., the wider the slit, the less resolution). The object was translated at right angles to the illuminating x-ray "fan" in 103 steps of 150 μm, as shown in Fig. 1. The sagittal scatter images were stacked and the transaxial images computed for ROI material analysis. An additional scatter imaging system located in the mirror-image location on the other side of the specimen would double the data collection efficiency.

The spatial resolutions in the three directions are determined by three mechanisms, besides factors such as divergence of the collimator, spectral resolution of x-ray source, etc. In the x direction, which is the translation direction of the object, as shown in Fig. 1, the resolution is determined by the translation step size and the beam "thickness." In the y direction, which is in the cross section of the beam and the object, as shown in Fig. 1, it is determined by the divergence of the collimator channel, the distance of the collimator to the object, and the detector resolution. In the z direction (i.e., the illuminating beam direction), the resolution depends on the relative orientation of the detector to the scattered rays. By having the imaging array at right angles to the collimated scatter rays (Fig. 1), the detector array pixel (diameter of 20 μm) projects to a rectangular pixel w wide and is equal to $d/\sin(\theta)$, where d is the pixel dimension of the detector and θ is the angle of the collimator to the illuminating x-ray beam (the coherent scatter angle). This greatly reduces the spatial resolution within the transaxial plane, especially at low angles. If the imaging array is positioned parallel to the x-ray beam, the resolution is not affected by the scatter angle. However, this presents some collimator/detector interfacing challenges. In our experiment, the detector and the collimator are oriented perpendicular to the scatter rays for easier alignment.

While the spatial dispersive approach of measuring the coherent scatters has mechanical challenges, a less mechanical challenging approach is to use polychromatic x-ray illumination and an energy dispersive array detector. We have at least partially demonstrated the feasibility by using x-ray sources with three different x-ray tube anode/filter combinations. With the technical development in high sensitivity and energy dispersive array detector, e.g., the CZT (CdZnTe) detector,[30,31] that approach is likely to be well suited to measuring the coherent scatter profile using bremsstrahlung x-ray exposure as this would provide the range in x-ray photon energies at each voxel using only a single angle of view.

Despite the technical challenges, it seems that the method can be best applied to detecting the presence or absence of

known materials that are essentially indistinguishable from each other or from tissue by virtue of their very similar x-ray attenuation coefficients.

V. CONCLUSION

In summary, we have explored the feasibility of discriminating and imaging the biocompatible materials in small objects with a test phantom with the presented method of three-dimensional coherently scattered x-ray imaging. The preliminary coherent scatter images at different scatter angles suggest that tissue scaffolds or biotissues with low attenuation contrast can be imaged with coherent x-ray scatter and sufficient contrast can be obtained at proper scatter angles with this method, which is difficult in the traditional attenuation CT imaging. It is possible to track and map the fate (e.g., its breakdown and/or removal) of specific components within tissue scaffolds to characterize the solute transport phenomena in biological systems including porous media such as tissue scaffolds, microvascular tree, etc. This experimental setup method is relatively easy to implement for coherent scatter x-ray imaging. Given sufficient x-ray intensity, the spatial resolution is determined by the array detector pixel size and the collimator channel size, which make it possible to image small specimens with micrometer or submillimeter resolution with the commercially available techniques.

ACKNOWLEDGMENT

This work was supported, in part, by NIH Grant No. EB000305. The authors do not have any conflict of interest to report.

[a]Author to whom correspondence should be addressed. Electronic mail: elran@mayo.edu; Telephone: 507 255 1933; Fax: 507 255 1935.

[1]J. A. Seibert and J. M. Boone, "X-ray imaging physics for nuclear medicine technologists. Part 2: X-ray interactions and image formation," J. Nucl. Med. Technol. **33**, 3–18 (2005).
[2]J. J. Curry, "Monte Carlo simulation of photon scattering in x-ray absorption imaging of high-intensity discharge lamps," J. Phys. D: Appl. Phys. **43**, 234001 (2010).
[3]J.-P. Schlomka, J. Delfs, H. Barschdorf, A. Thran, and U. Van Stevendaal, "Experimental feasibility study of energy resolved fan-beam coherent scatter computed tomography," Proc. SPIE **5535**, 410–423 (2004).
[4]J. A. Grant, M. J. Morgan, J. R. Davis, D. R. Davies, and P. Wells, "X-ray diffraction microtomography," Meas. Sci. Technol. **4**, 83–87 (1993).
[5]V. Pecharsky and P. Zavalij, *Fundamentals of Powder Diffraction and Structural Characterization of Materials*, 2nd ed. (Springer, New York, 2008).
[6]D. Blow, *Outline of Crystallography for Biologists* (Oxford University Press, Oxford, 2002).
[7]J. Kosanetzky, B. Knoerr, G. Harding, and U. Neitzel, "X-ray diffraction measurements of some plastic materials and body tissues," Med. Phys. **14**(4), 526–531 (1987).
[8]M. S. Westmore, A. Fenster, and I. A. Cunningham, "Tomographic imaging of the angular dependant coherent scatter cross section," Med. Phys. **24**, 3–10 (1997).
[9]M. C. Poletti, O. D. Goncalves, and I. Mazzaro, "X-ray scattering from human breast tissues and breast-equivalent materials," Phys. Med. Biol. **47**(1), 47–63 (2002).
[10]G. Harding, "X-ray scatter tomography for explosives detection," Radiat. Phys. Chem. **71**(3–4), 869–881 (2004).
[11]H. Jin *et al.*, "High resolution three dimensional visualization and characterization of coronary atherosclerosis by synchrotron and highly localized x-ray diffraction," Phys. Med. Biol. **47**, 4345–4356 (2002).
[12]D. L. Batchelar, M. T. M. Davidson, W. Dabrowski, and I. A. Cunningham, "Bone composition imaging using coherent-scatter computed tomography. Assessing bone health beyond bone mineral density," Med. Phys. **33**(4), 904–915 (2006).
[13]M. De Felici, R. Felici, C. Ferrero, A. Tartari, M. Gambaccini, and S. Finet, "Structural characterization of the human cerebral myelin sheath by small angle x-ray scattering," Phys. Med. Biol. **53**(20), 5675–5688 (2008).
[14]G. Martens, H. Bomsdorf, G. L. Harding, J. Kanzenbach, and R. Linde, "Coherent x-ray scatter imaging for food-stuff contamination detection," Proc. SPIE **2092**, 387–398 (2009).
[15]A. Hoshino, T. Takeda, M. Akiba, T. Kazama, Y. Watanabe, T. Yuasa, K. Hyodo, A. Uchida, T. Akatsuka, and Y. Itai, "A coherent scatter computed tomography with scintillator-CCD system," Proceedings of the 18th Annual International Conference of the IEEE: Engineering in Medicine and Biology Society, Amsterdam, 1996, Vol. 2, pp. 726–727, 1996 (unpublished).
[16]D. L. Batchelar and I. A. Cunningham, "Material-specific analysis using coherent-scatter imaging," Med. Phys. **29**(8), 1651–1660 (2002).
[17]S. M. Schneider, J.-P. Schlomka, and G. L. Harding, "Coherent-scatter computed tomography applying a fan-beam geometry," Proc. SPIE **4320**, 754–763 (2001).
[18]A. Harding, J.-P. Schlomka, and G. L. Harding, "Simulations and experimental feasibility study of fan-beam coherent-scatter CT," Proc. SPIE **4786**, 202–209 (2002).
[19]J.-P. Schlomka, A. Harding, U. van Stevendaal, M. Grass, and G. L. Harding, "Coherent scatter computed tomography: A novel medical imaging technique," Proc. SPIE **5030**, 256–265 (2003).
[20]U. vanStevendaal, J. P. Schlomka, A. Harding, and M. Grass, "A reconstruction algorithm for coherent scatter computed tomography based on filtered back-projection," Med. Phys. **30**(9), 2465–2474 (2003).
[21]W. Zhou and C. A. MacDonald, "Diffraction imaging with conventional sources," Proc. SPIE **7077**, 70770K (2008).
[22]C. A. MacDonald and W. M. Gibson, "Medical applications of polycapillary x-ray optics," Proc. SPIE **2519**, 186–196 (1995).
[23]G. Margaritondo, *Introduction to Synchrotron Radiation* (Oxford University Press, New York, 1988), p. 280.
[24]S. M. Jorgensen, D. A. Reyes, C. A. MacDonald, and E. L. Ritman, "Micro-CT scanner with a focusing polycapillary x-ray optic," Proc. SPIE **37772**, 158–166 (1999).
[25]P. A. Ross, "A new method of spectroscopy for faint x-radiations," J. Opt. Soc. Am. **16**, 433–437 (1928).
[26]L. R. M. Morin, "Molecular form factors and photon coherent scattering cross sections of water," J. Phys. Chem. **11**, 1091–1098 (1982).
[27]C.-W. Cui, S. M. Jorgensen, D. R. Eaker, and E. L. Ritman, "Coherent x-ray scattering for discriminating bio-compatible materials in tissue scaffolds," Proc. SPIE **7078**, 70781S-1–70781S-10 (2008).
[28]R. A. de Kemp, F. H. Epstein, C. Catana, B. M. W. Tsui, and E. L. Ritman, "Small-animal molecular imaging methods," J. Nucl. Med. **51**, 18S–32S (2010).
[29]S. M. Jorgensen, O. Demirkaya, and E. L. Ritman, "Three dimensional imaging of vasculature and parenchyma in intact rodent organs with x-ray micro-CT," Am. J. Physiol. **44**, H1103–H1114 (1998).
[30]L. Verger, A. Drezet, E. G. d'Aillon, C. Mestais, O. Monnet, G. Montemont, F. Dierre, and O. Peyret, "New perspectives in gamma-ray imaging with CdZnTe/CdTe," IEEE Nuclear Science Symposium Conference Record, Vol. 4, pp. 2313–2319, 2004 (unpublished).
[31]A. A. Bulycheva, I. E. Tsirkunova, and V. V. Gostilo, "CdZnTe pixel detectors for medical imaging," IFMBE Proceedings: 14th Nordic-Baltic Conference on Biomedical Engineering and Medical Physics, Riga, Latvia, June 16–20, 2008, Vol. 20, pp. 477–480, 2008 (unpublished).